Three-magnon excitations in ferromagnetic spin-S chains

1994 J. Phys.: Condens. Matter 6 10075

(http://iopscience.iop.org/0953-8984/6/46/024)

J. Phys.: Condens. Matter 6 (1994) 10075–10092. Printed in the UK

Three-magnon excitations in ferromagnetic spin-S chains

B W Southern†, R J Lee† and D A Lavis‡

† Department of Physics, University of Manitoba, Winnipeg, Manitoba, Canada R3T 2N2
‡ Department of Mathematics, King's College, The Strand, London WC2R 2LS, UK

Received 27 June 1994

Abstract. The nature of three-magnon excitations in general spin-S quantum spin chains is studied using the recursion method. The asymptotic behaviour of the recurrence coefficients can be used to identify the presence of bound states in the spectrum. Special features of integrable models are easily identified.

1. Introduction

Generalized Heisenberg spin chains with general spin S provide excellent opportunities to study the nature of excitations in both integrable and non-integrable systems. Bethe [1] first showed how to obtain the eigenvalues and eigenvectors of the $S = \frac{1}{2}$ Heisenberg chain using a method which is now called the Bethe *ansatz*. This same approach can also be used for more general $S > \frac{1}{2}$ models which have a permutation symmetry [2, 3]. More recently, the Bethe *ansatz* has been related to the quantum inverse scattering method [4] and the nature of excitations in both ferromagnets and antiferromagnets has been investigated. This has been followed by the identification [5, 6, 7, 8] of other $S > \frac{1}{2}$ integrable models. In general, the excitations can be classified according to their total wavevector K and their total $S^Z = NS - m$ and are referred to as m-magnon excitations. Bethe's results showed that for $m > 1$ the excitations can be of two types: scattering states and bound states.

For the ferromagnetic case, the vacuum state has all spins aligned parallel and the complete excitation spectrum consists of both bound states and resonant states within the continuum of scattering states. However, the nature of excitations in the antiferromagnetic case has been more controversial. In the case of the integrable models, the low-energy excitations from the antiferromagnetic vacuum are gapless two-particle scattering states and bound states do not exist at any value of S. The non-integrable models were expected to have similar properties until the work of Haldane [9] predicted that the excitations for integer values of S have a gap whereas for half-integer values there is no gap. The nature of bound states in the antiferromagnetic case remains unresolved.

In the case of a ferromagnetic ground state, the one-magnon and two-magnon problems can be solved exactly [10]. However, most investigations of the m-magnon problem for $m > 2$ have been restricted to the integrable models. Haldane [11] considered the ferromagnetic vacuum and has suggested that the bound and resonant type of m-magnon states form $p = \min(m, 2S)$ branches in the general model and that all branches are real and continuous across p Brillouin zones in an extended zone scheme for the integrable models. In the non-integrable models, the branches enter the continuum and gaps occur at the Brillouin zone boundaries. Chubukov and Kveschenko [12] studied the two-magnon

0953-8984/94/4610075+18$19.50

problem for $S = 1$ and $S = \frac{3}{2}$ and used this criterion for the absence of gaps to identify integrable models. However, as we shall demonstrate, one needs to study the $2S$-magnon problem to ensure integrability.

There have been relatively few papers which have considered three-magnon excitations in the past. The studies of Majumdar [13, 14, 15] and Van Himbergen [16] were based on the formalism developed by Faddeev [17], which treats the system in terms of spin waves which can scatter off one another or bind together to form a stable complex. In these studies the approach to the problem is very general but detailed solutions are given only for a one-dimensional spin-$\frac{1}{2}$ chain. In addition, it is difficult to identify non-physical states such as those which correspond to raising a single spin by more than $2S$ and spurious solutions can appear. Another study which posed the problem in a slightly different form (but using a similar method of solution) was that by Millet and Kaplan [18]. These authors considered a spin-S model and also encountered a spurious solution for $S = \frac{1}{2}$. Systems with $S > \frac{1}{2}$ were studied without such difficulties but results were obtained only for Heisenberg systems.

In the present work we describe a method to calculate three-magnon excitations in ferromagnets. Our approach to the three-magnon problem maps it exactly onto an effective tight-binding Hamiltonian. General properties are easily extracted for the most general isotropic spin Hamiltonian for spin S. The special cases which correspond to completely integrable models are identified with special properties of the three-magnon excitations in agreement with Haldane. In the next section we describe the general S-model and outline our method of solution. Our results for the three-magnon excitation spectrum of various spin-S models are given in section 3.

2. The model

We consider the following Hamiltonian for a chain of spin-S quantum spins

$$\widehat{\mathcal{H}} = -\sum_{i=1}^{N}\sum_{n=1}^{2S} J^{(n)}(S_i \cdot S_{i+1})^n. \tag{1}$$

The interactions are restricted to nearest neighbours but further neighbours can also be included as well as various types of anisotropies without difficulty. The Hamiltonian in (1) is the most general form for spin S with SU(2) symmetry. The model with only the $n = 1$ term is the usual Heisenberg model. The special cases which are completely integrable correspond to particular values of the $J^{(n)}$.

However, rather than use the $J^{(n)}$, we will use certain linear combinations which are most easily described by considering an isolated pair of nearest-neighbour spins. The total angular momentum j of the pair can take the values $j = 0, 1, ..., 2S$ and the energy eigenvalue of the pair in state j is

$$\lambda_j = -\sum_{n=1}^{2S} J^{(n)}[j(j+1)/2 - S(S+1)]^n. \tag{2}$$

It is convenient to define the eigenvalues with respect to the state of maximum j and ratios of these quantities as follows:

$$\begin{aligned} \alpha_m(S) &= \lambda_{2S-m} - \lambda_{2S} \\ g_m(S) &= \frac{\alpha_m(S)}{\alpha_1(S)} \end{aligned} \tag{3}$$

where $m = 0, 1, ..., 2S$. Note that $g_0(S) = 0$ and $g_1(S) = 1$ for all values of the $J^{(n)}$ in (1). The advantage of using the $g_m(S)$ rather than the $J^{(n)}$ is that the m-magnon problem only involves the first m of the former combinations.

The known integrable cases correspond to the following choices of the $g_m(S)$: the values of the $J^{(n)}$ which yield the Schrödinger [2] exchange operator for general S correspond to

$$g_m(S) = \frac{1-(-1)^m}{2}. \tag{4}$$

The values of the $J^{(n)}$ of Takhtajan [5] and Babujian [6] correspond to

$$g_m(S) = 2S[\psi(2S+1) - \psi(2S+1-m)] \tag{5}$$

where ψ is the derivative of the logarithm of the gamma function. This model is integrable but still has SU(2) symmetry. The case corresponding to $\alpha_{2S} = 1$ with all remaining $\alpha_m = 0$ has been investigated by Batchelor and Barber [8]. They show that this corresponds to an integrable model which satisfies the Temperly–Lieb algebra of the $(2S+1)^2$-state Potts model. Finally, the Heisenberg model for general S corresponds to

$$g_m(S) = m(4S+1-m)/4S. \tag{6}$$

In the following, we assume that the ground state of (1) corresponds to the ferromagnetic state $|0\rangle$ with all spins aligned along the negative z direction. The one-magnon eigenstates are plane waves with excitation energy

$$E_1 = \alpha_1(S)[1-\cos(K)]. \tag{7}$$

Hence the one-magnon energy is the same for all choices of the $J^{(n)}$ when the energy is measured in units of $\alpha_1(S)$. For stability of the ground state with respect to one-magnon excitations we require $\alpha_1(S)$ to be non-negative. The two-magnon spectrum of the general Hamiltonian (1) has been studied [19, 20] recently using a real-space rescaling approach. The solutions depend upon the value of $g_2(S)$ with the excitations of the integrable models having special features. However, these properties are independent of the values of the remaining $g_m(S)$ for $S > 1$. Hence an $S = \frac{3}{2}$ model may have features in its two-magnon spectrum which suggest integrability but the three-magnon spectrum will not necessarily have the same features since it depends on the value of $g_3(S)$ as well.

The three-magnon excitations are solutions of the Schrödinger equation which can be written in the basis of three-spin deviation states

$$|r, l, m\rangle = S_r^+ S_l^+ S_m^+ |0\rangle \qquad (r \leqslant l \leqslant m). \tag{8}$$

Using centre of mass and relative coordinates for the sites r, l and m, we can express the Hamiltonian in a mixed orthonormal basis $|K; x, y\rangle$, where K represents the total wavevector of the three-magnon state and $x = |l-r|$ and $y = |m-l|$ represent the relative separation of the spin deviations in units of the lattice spacing a. In this mixed basis the

Schrödinger equation can be expressed in the following tight-binding form:

$$
\begin{aligned}
(E-\varepsilon)|K;x,y\rangle &= V^*|K;x+1,y\rangle + V|K;x-1,y\rangle + V^*|K;x-1,y+1\rangle \\
&\quad + V|K;x+1,y-1\rangle + V^*|K;x,y-1\rangle + V|K;x,y+1\rangle \\
(E-\varepsilon_4)|K;x,1\rangle &= V^*|K;x+1,1\rangle + V|K;x-1,1\rangle + V^*|K;x-1,2\rangle \\
&\quad + V|K;x,2\rangle + W^*|K;x,0\rangle + W|K;x+1,0\rangle \\
(E-\varepsilon_4)|K;1,y\rangle &= V^*|K;1,y-1\rangle + V|K;1,y+1\rangle + V^*|K;2,y\rangle \\
&\quad + V|K;2,y-1\rangle + W^*|K;0,y+1\rangle + W|K;0,y\rangle \\
(E-\varepsilon_2)|K;1,1\rangle &= V^*|K;2,1\rangle + V|K;1,2\rangle + W^*|K;1,0\rangle \\
&\quad + W|K;0,1\rangle + W^*|K;0,2\rangle + W|K;2,0\rangle \\
(E-\varepsilon_3)|K;x,0\rangle &= V_1^*|K;x+1,0\rangle + V_1|K;x-1,0\rangle \\
&\quad + W^*|K;x-1,1\rangle + W|K;x,1\rangle \\
(E-\varepsilon_3)|K;0,y\rangle &= V_1^*|K;0,y-1\rangle + V_1|K;0,y+1\rangle \\
&\quad + W^*|K;1,y\rangle + W|K;1,y-1\rangle \\
(E-\varepsilon_1)|K;1,0\rangle &= U^*|K;0,1\rangle + V_1^*|K;2,0\rangle + W|K;1,1\rangle + V_0|K;0,0\rangle \\
(E-\varepsilon_1)|K;0,1\rangle &= U|K;1,0\rangle + V_1|K;0,2\rangle + W^*|K;1,1\rangle + V_0^*|K;0,0\rangle \\
(E-\varepsilon_0)|K;0,0\rangle &= V_0^*|K;1,0\rangle + V_0|K;0,1\rangle
\end{aligned}
\tag{9}
$$

where the energy E is measured relative to the ferromagnetic ground state $E_0 = N\lambda_{2S}$ and both x and y are $\geqslant 2$.

The various parameters appearing in the equations above are given by

$$
\begin{aligned}
\varepsilon_0 &= 3S(S-1)\left[\frac{\alpha_1(S)\,[1-\cos(K)]}{S(4S-3)} + \frac{\alpha_2(S)\,[1+\cos(K)]}{(S-1)(4S-1)} + \frac{\alpha_3(S)\,[1-\cos(K)]}{3(S-1)(4S-3)}\right] \\
\varepsilon_1 &= \frac{1}{2}\left[\frac{3(3S-2)\alpha_1(S)}{(4S-3)} + \frac{(3S-1)\alpha_2(S)}{(4S-1)} + \frac{3(S-1)\alpha_3(S)}{(4S-3)}\right] \\
\varepsilon_2 &= \alpha_1(S) + 2\left(\frac{2S-1}{4S-1}\right)\alpha_2(S) \\
\varepsilon_3 &= 2\alpha_1(S) + \frac{2S}{(4S-1)}\alpha_2(S) \\
\varepsilon_4 &= 2\alpha_1(s) + \left(\frac{2S-1}{4S-1}\right)\alpha_2(S) \\
\varepsilon &= 3\alpha_1(S) \\
V_0 &= \frac{1}{2}\zeta\sqrt{3S(S-1)}\left[\frac{\alpha_1(S)(1-\zeta^{*3})}{(4S-3)} - \frac{\alpha_2(S)(1+\zeta^{*3})}{(4S-1)} - \frac{\alpha_3(S)(1-\zeta^{*3})}{(4S-3)}\right] \\
U &= -\frac{1}{2}\zeta\left[\frac{S\alpha_1(S)}{(4S-3)} + \frac{(1-S)\alpha_2(S)}{(4S-1)} - \frac{3(1-S)\alpha_3(S)}{(4S-3)}\right] \\
V_1 &= -\frac{1}{2}\zeta\left[\alpha_1(S)(1+\zeta^{*3}) - \frac{2S\zeta^{*3}\alpha_2(S)}{(4S-1)}\right] \\
W &= -\zeta\alpha_2(S)\frac{\sqrt{S(2S-1)}}{(4S-1)} \\
V &= -\frac{1}{2}\zeta\alpha_1(S)
\end{aligned}
\tag{10}
$$

where $\zeta = \exp(\mathrm{i}K/3)$ and the wavevector K lies in the range $-\pi \leqslant K \leqslant \pi$. The above equations can be represented graphically as shown in figure 1.

The system corresponds to a semi-infinite triangular lattice with a surface along the positive x and y axes. These surfaces describe states where two deviations are on the same site and the origin corresponds to the state with three deviations on the same site. The effective tight-binding Hamiltonian has six different types of diagonal terms ($\varepsilon_0, \varepsilon_1, \varepsilon_2, \varepsilon_3, \varepsilon_4, \varepsilon$) and five different types of coupling (V_0, U, W, V, V_1). All are functions of S, K, g_2 and g_3 and the off-diagonal terms are complex functions of K.

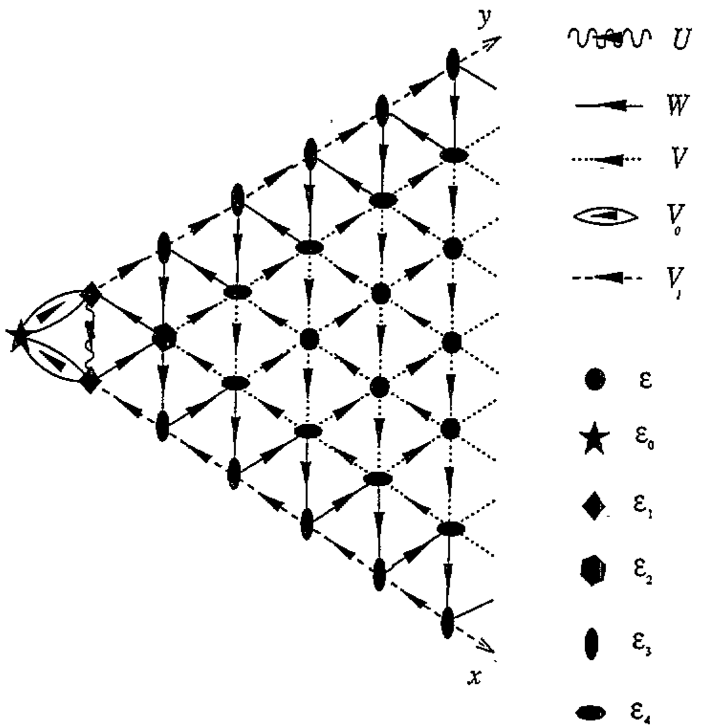

Figure 1. Graphical representation of the general three-magnon Hamiltonian acting on states $|K; x, y\rangle$.

The site coordinates label the values of x and y in the ket $|K; x, y\rangle$ and the lines connecting the sites represent the interactions between kets. The arrows indicate that the interactions are complex. When the Hamiltonian acts on the ket at any site, it yields a linear combination of up to seven kets. These kets include the one acted upon and the six nearest neighbours. The coefficient of the self-term is the appropriate ε for that site and the coefficients of the neighbouring kets are the interaction parameters (U, W, V, V_0, V_1) corresponding to the type of line connecting the neighbours. If the arrow on the line is pointing towards the site acted upon, then the complex conjugate of the interaction should be taken.

A simple example can be read off the figure as follows: suppose the effect of $\widehat{\mathcal{H}}$ on $|K; 1, 1\rangle$ is desired. Since $|K; 1, 1\rangle$ is equivalent to $(x, y) = (1, 1)$ on the diagram the self-term involves ε_2. The interaction lines connect this site to $(1, 2)$, $(2, 1)$ and $(0, 1)$, $(1, 0)$, $(2, 0)$, $(0, 2)$ which correspond to the interactions V and W respectively. Half of the arrows point towards (1, 1) and hence the net effect is

$$\begin{aligned}\widehat{\mathcal{H}}|K;1,1\rangle &= \varepsilon_2|K;1,1\rangle + V^*|K;2,1\rangle + V|K;1,2\rangle + W^*|K;1,0\rangle\\ &\quad + W|K;0,1\rangle + W^*|K;0,2\rangle + W|K;2,0\rangle\end{aligned}$$

as given in (9).

For $S=\frac{1}{2}$, the system of equations represented by figure 1 separates into two groups of states. Since the x and y coordinates represent the separation of the spin deviations, clearly the edges and the apex at the left are unphysical as these have x and/or y equal to zero and correspond to a single spin being raised by more than one deviation. When the parameters which describe the Hamiltonian (ε_0, ε_1, $\cdots$, ε_4, ε, V_0, V_1, V, U, W) are evaluated, the unphysical layer completely decouples from the rest. Graphically, this unphysical Hamiltonian takes the form shown in figure 2.

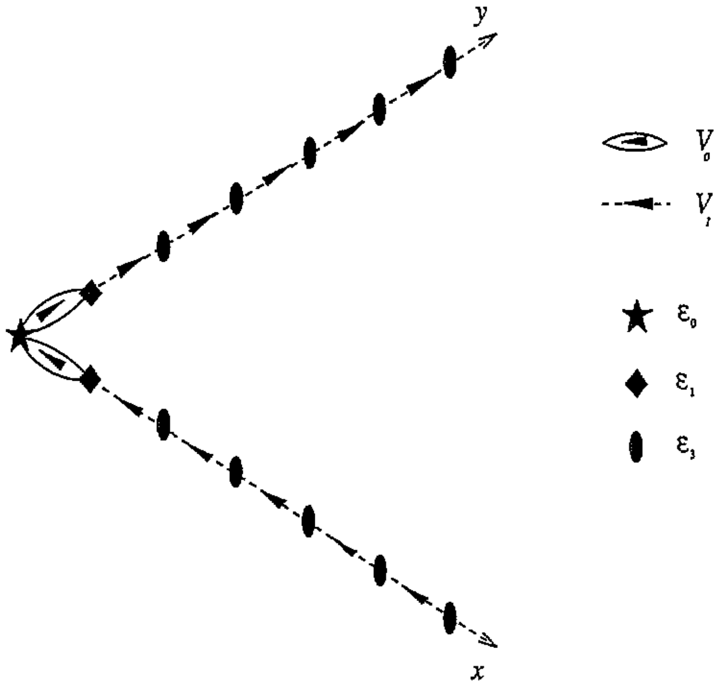

Figure 2. Graphical representation of the unphysical part of the three-magnon Hamiltonian for $S=\frac{1}{2}$.

The equations for these 'surface' states contain an unphysical solution $E=\frac{7}{8}$ which is independent of K. This solution was also found in previous studies [18] of the $S=\frac{1}{2}$ model but was difficult to eliminate. In our approach, these unphysical states are clearly identified. The remaining 'bulk' states are the physical states and the solutions correspond to those found by Bethe [1].

Before we describe our general approach to solving these equations, we will first consider the $S>\frac{1}{2}$ integrable cases. When the g_m have the values corresponding to (4), the Hamiltonian has SU($2S+1$) symmetry and there is again a decoupling of the states with two deviations on the same site from the rest as shown in figure 3. In addition, the state with three deviations on the same site is also completely decoupled and the corresponding solution for the energy $E=\varepsilon_0=\alpha_1(S)\,(1-\cos(K))$ is degenerate with the one-magnon

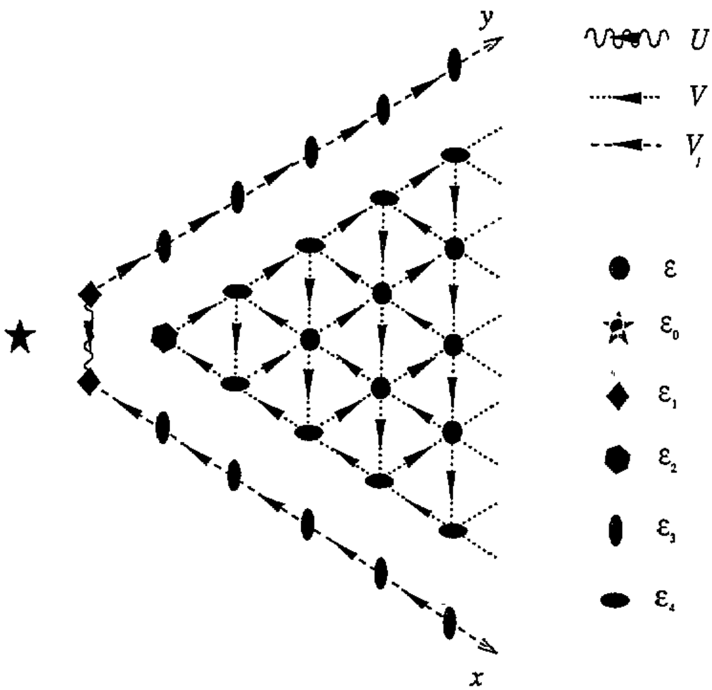

Figure 3. Graphical representation of the SU($2S+1$) three-magnon Hamiltonian.

energy. This state is of course unphysical for $S \leqslant 1$. The equations for the states with two deviations on the same site can be written in the form of a semi-infinite chain and have solutions which are identical to the two-magnon spectrum of the $S = \frac{1}{2}$ model but with the energy mutliplied by $\alpha_1(S)$: there are scattering-state solutions in the range

$$2\alpha_1\left(1-\cos\left(\frac{K}{2}\right)\right) \leqslant E \leqslant 2\alpha_1\left(1+\cos\left(\frac{K}{2}\right)\right)$$

and a two-magnon bound-state solution with $E = \frac{1}{2}\alpha_1(1-\cos(K))$. The remaining 'bulk' equations are identical to the $S = \frac{1}{2}$ case and the solutions have the same form as that found by Bethe for $m = 3$ with all energies scaled by $\alpha_1(S)$: there are scattering states of three free magnons which form a continuum in the range

$$3\alpha_1\left(1-\cos\left(\frac{K}{3}\right)\right) \leqslant E \leqslant 3\alpha_1\left(1-\cos\left(\frac{2\pi+K}{3}\right)\right)$$

as well as a two bound/one free continuum in the range

$$\alpha_1\left(\frac{3}{2}-\sqrt{\frac{5}{4}+\cos(K)}\right) \leqslant E \leqslant \alpha_1\left(\frac{3}{2}+\sqrt{\frac{5}{4}+\cos(K)}\right).$$

These two continua overlap with the three free giving the maximum energy at any K and the two bound/one free giving the minimum energy. There is also a three-magnon bound state below these continua with energy $E = \frac{1}{3}\alpha_1(1-\cos(K))$. Thus the following general pattern emerges for this integrable case of SU($2S+1$) symmetry: for the general m-magnon problem the system decouples into separate groups of equations for the states involving $n = 1, 2, \ldots, m$ deviations on a single site. Each of these groups has solutions identical to the $(m-n+1)$-magnon spectrum of the $S = \frac{1}{2}$ model. The SU(2) integrable case given by (5) does not yield a decoupling of the basis kets and must be investigated directly using the method decribed below.

In order to obtain information about the spectral properties of the general Hamiltonian in (1), we have used the recursion method [21] to transform this triangular system to a semi-infinite chain. This provides a continued-fraction representation of the local Green's function which can easily be used to calculate the local density of states. The method is based on a three-term recursion relation of the form

$$\widehat{\mathcal{H}}u_n = a_n u_n + b_{n+1}u_{n+1} + b_n u_{n-1} \tag{11}$$

where $a_n, b_n \in \mathcal{R}$ and u_n is the nth state of an arbitrary complete orthonormal set of states. To start the procedure, we define $u_{-1} \equiv 0$ and choose some arbitrary normalized state vector u_0. A second normalized state vector, u_1, is obtained from

$$\widehat{\mathcal{H}}u_0 = a_0 u_0 + b_1 u_1. \tag{12}$$

Taking u_1 to be orthogonal to u_0 it follows that

$$a_0 = u_0^\dagger \widehat{\mathcal{H}} u_0 \tag{13}$$

$$b_1 u_1 = \widehat{\mathcal{H}}u_0 - a_0 u_0 \tag{14}$$

where b_1 is the normalization factor for u_1. Once we have the first two vectors, we can use (11) to generate the rest. In general, (14) is replaced by

$$b_{n+1}u_{n+1} = \widehat{\mathcal{H}}u_n - a_n u_n - b_n u_{n-1}$$

where b_{n+1} is the normalization factor for u_{n+1}. By iterating this procedure, the set of vectors $\{u_n\}$, can be found which will transform the Hamiltonian to the desired canonical form and the resulting tridiagonal matrix will contain the a_n and b_n as its elements. In the new basis the Hamiltonian satisfies

$$\widehat{\mathcal{H}}\begin{pmatrix} u_0 \\ u_1 \\ u_2 \\ \vdots \end{pmatrix} = \begin{bmatrix} a_0 & b_1 & & & \\ b_1 & a_1 & b_2 & & 0 \\ & b_2 & a_2 & b_3 & \\ & & 0 & & \ddots \end{bmatrix} \begin{pmatrix} u_0 \\ u_1 \\ u_2 \\ \vdots \end{pmatrix} \tag{15}$$

and corresponds to an inhomogeneous nearest-neighbour tight-binding chain.

If we take the lattice shown in figure 1 and consider the columns of sites with the same index $n = x + y$, then for any choice of initial ket in the three-magnon basis, $u_0 = |K; x, y\rangle$, each successive application of the above procedure can only couple to the kets in neighbouring columns. For example, if $u_0 = |K; 0, 0\rangle$, then after the first iteration, u_1 involves the kets $|K; 1, 0\rangle$ and $|K; 0, 1\rangle$. The second iteration yields a u_2 which can involve some combination of $|K; 1, 0\rangle$ and $|K; 0, 1\rangle$, which is linearly independent from u_1, as well as terms involving $|K; 2, 0\rangle$, $|K; 0, 2\rangle$ and $|K; 1, 1\rangle$. The new state formed at each iteration is constructed to be orthogonal to the previous two states, and thus only these two states need be stored to find the next basis state . The precise values of the a_n and b_n generated will depend upon the choice of initial ket.

For the infinite system of equations represented by figure 1, the recursion process continues indefinitely and this raises the question of when and how to stop the procedure. There are a number of possibilities [22, 23, 24] for the behaviour of the coefficients a_n and b_n as a function of n. The coefficients may approach constants, approach some kind of periodic oscillations or behave in a more complicated fashion. The asymptotic form for the coefficients is determined by the scattering states of the spectrum. If these states are composed of overlapping continua with no gaps, then the coefficients approach constant values which are determined by the maximum and minimum values of the overlaping continua. For the three-magnon case, these continua have energies equal to either the sum of 3 free magnons or two bound and one free. For $S > \frac{1}{2}$ there can be more than one two-magnon bound-state branch and there is a continuum corresponding to each branch. If the superposition of the continua leads to internal gaps in the continuum, then the asymptotic form of the coefficients can be more complicated [24] and will depend upon the values of the energies at the edges of the gaps as well. In each case, once the asymptotic behaviour is reached, the iteration process can be terminated and the remaining coefficients can be obtained using the asymptotic form. In our case, knowledge of the complete two-magnon spectrum is all that is required to predict this behaviour.

As an illustration of the method, we will first consider the case of $S = \frac{1}{2}$ where our Hamiltonian reduces to the case solved by Bethe. Since each ket in our initial ket space is labelled by the total wavevector $\boldsymbol{K}$, we carry out the procedure for fixed $\boldsymbol{K}$. When the recursion method is applied to any state contained within the physical part of the Hamiltonian the resulting coefficients rapidly converge (~ 20 iterations) to nearly constant values. However, internal Van Hove singularities in the three free or two bound/one free magnon continua may produce visible oscillations [22] which are still noticeable at this stage. It is therefore necessary to continue the method well beyond 20 iterations to reach the asymptotic form.

For the $S = \frac{1}{2}$ case, the asymptotic values of the coefficients a_n and b_n are determined as follows:

$$\begin{aligned} a_n &\to (E_{\max} + E_{\min})/2 \\ b_n &\to (E_{\max} - E_{\min})/4 \end{aligned} \tag{16}$$

where $E_{\max}$ and $E_{\min}$ are the maximum and minimum energies of the scattering-state solutions and are given by

$$\begin{aligned} E_{\max} &= 3\left\{1 - \cos\left(\frac{2\pi + K}{3}\right)\right\} \\ E_{\min} &= \left\{\frac{3}{2} - \sqrt{\frac{5}{4} + \cos(K)}\right\}. \end{aligned} \tag{17}$$

Hence, at $K = \pi$, the coefficients a and b should approach the values 3.5 and 1.25 respectively.

The a_n, b_n generated by the recursion method with 285 iterations at $K = \pi$ are shown in figure 4 using the initial choice of ket $u_0 = |K; 1, 1\rangle$. There are significant variations in the coefficients initially but they appear to approach the expected limiting values after ~ 30 iterations. However, as the procedure is continued further, the coefficients exhibit anomalously large deviations from the values to which the coefficients should converge. For example, using single-precision calculations in Fortran 77 the anomalous deviations repeat fairly regularly with a period of approximately 34 iterations and the first appears at the 38th iteration. However, these deviations can be shown to be strictly numerical in origin by calculating the recursion coefficients at various precisions. By changing to double-precision, the first deviation does not appear until the 77th iteration and the period of repetition is almost exactly double at 67 as shown in figure 5. Performing the calculation at quadruple precision moves the first deviation to the 152nd iteration.

At a first glance, this behaviour appears to be an unusual case of oscillations in the coefficients, which normally indicates a gap in the continuum [24]. The exact solutions [1]

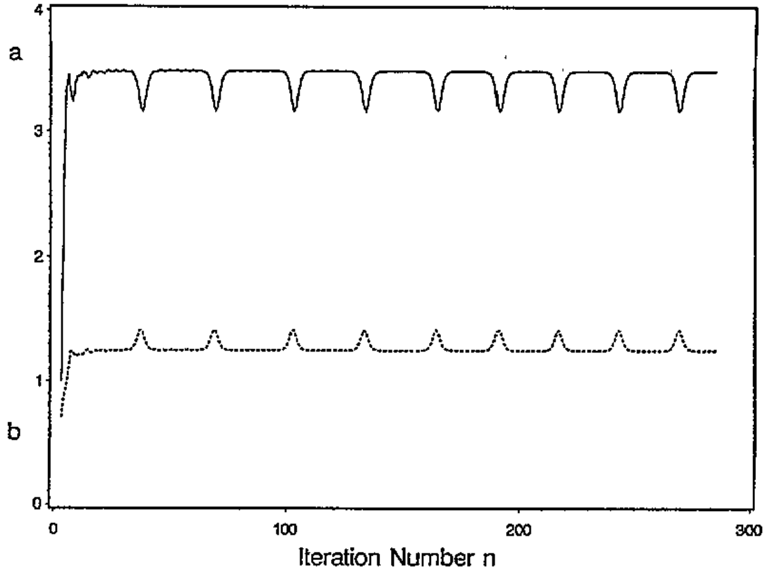

Figure 4. Single-precision coefficients a_n, b_n for $S = \frac{1}{2}$ at $K = \pi$.

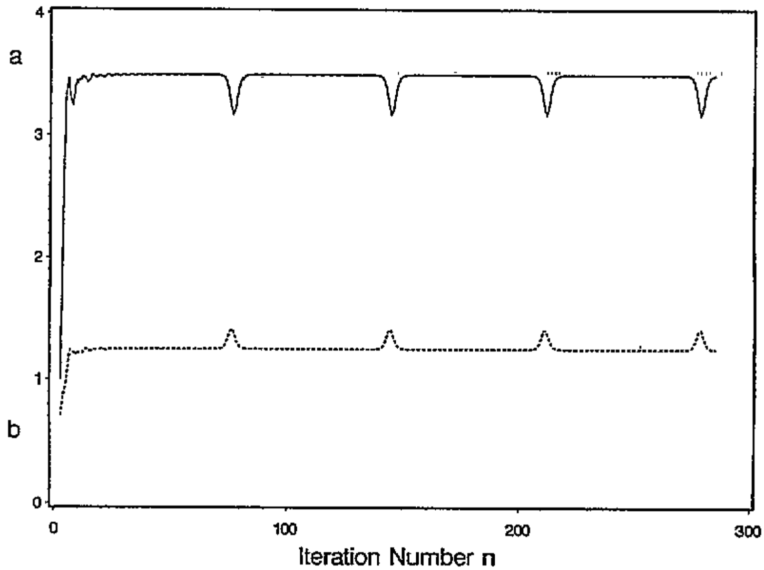

Figure 5. Double-precision coefficients a_n, b_n for $S = \frac{1}{2}$ at $K = \pi$.

do not exhibit any such gap, but we can imagine one to be present if the bound state below the continuum is treated not as a delta function, but as having a very narrow but finite width equal to the machine zero for each precision. In the case where real gaps are present, the asymptotic behaviour of the coefficients is described by hyperelliptic (or Abelian) functions [24, 26]. In the limit of narrow bands these functions tend to have relatively abrupt peaks or valleys separated by wide flat regions and are similar to soliton profiles [25]. The paper by Turchi *et al* [24] gives a detailed analysis of a band with one gap which requires knowledge of the energies of the edges for each band. In the present case, at $K = \pi$, the energies for the scattering-state band lie in the range 1 to 6 (in units of α_1) and there is a bound state at $\frac{2}{3}$. Taking the double-precision case and the machine accuracy to be approximately 10^{-14}, the energy bands extend from $(E_1, E_2) = (\frac{2}{3} - \frac{10^{-14}}{2}, \frac{2}{3} + \frac{10^{-14}}{2})$ and $(E_3, E_4) = (1, 6)$. The period for the index for the recursion coefficients, δn, is related to the ratio of two elliptic integrals evaluated over the regions outside the bands. Following the analysis in section 4.5 of the paper by Turchi *et al* [24], we obtain the value $\delta n = 67$ (for the nearest integer) which is in agreement with the observed period in figure 5. When the calculation is generalized to an arbitrary narrow band width, γ, centred on the bound-state energy, we find that $\delta n \propto -\ln(\gamma)$ and that the maximum (or minimum) of the deviations in the coefficients a_n is equal to the binding energy of the bound state. If the bound state is below the continuum, the deviations are negative, but if it is above, they are positive. Thus the asymptotic behaviour of the recursion coefficients gives direct evidence about the location of bound states.

Another method of analysis which supports the above interpretation is to study neigbouring pairs of the coefficients using phase space plots. Turchi *et al* [24] derived recurrence laws for the coefficients by examining the asymptotic form of the continued fraction. For a single gap, equation (4.29) of their paper shows that any pair of neighbouring coefficients $(A, B) = (a_n, b_{n-1}^2)$ or (a_n, b_n^2) satisfy

$$\left(A^2 + A_1 A + A_2 A + 2B\right)^2 = X(-A_1 - A) \tag{18}$$

where

$$\begin{aligned} A_1 &= -\frac{1}{2}\sum_{i=1}^{4} E_i \\ A_2 &= \frac{1}{2}\sum_{i<j} E_i E_j - \frac{1}{2}A_1^2 \\ X(x) &= \prod_{i=1}^{4}(E_i - x). \end{aligned} \tag{19}$$

Equation (18) can be viewed as a relation in the phase space of a_n and b_n^2 and is dependent upon the values used for the energies of the four band edges. A change to any of the energies can alter its graphical appearance significantly. A phase space plot is shown in figure 6 for our double-precision coefficient calculation. The solid line is obtained from (18), taking $E_1 = \frac{2}{3} - \frac{10^{-14}}{2}$, $E_2 = \frac{2}{3} + \frac{10^{-14}}{2}$, $E_3 = 1$ and $E_4 = 6$ and the two types of symbols represent $(a_n,\ b_n^2)$ and $(a_n,\ b_{n-1}^2)$ pairs. The first 50 coefficients have been ignored as the analysis is valid only in the asymptotic region.

The iterations where the coefficients are essentially constant appear at the lower right-hand corner whereas the deviations are distributed along the rest of the curve. The maximum deviations in A are 0.33 which is the energy difference between the lower edge of the scattering-state continuum and the three-magnon bound state.

The excellent agreement of the phase space plots with our calculated coefficients and our ability to predict the period and amplitude of the anomalous deviations are convincing arguments for regarding the deviations as simply due to numerical limitations of the computer system which was used. These limitations result in a non-zero width for the bound state but do not affect the energy of any bound state or band edges. Hence, these deviations can be ignored and the recursion coefficients can be replaced by their asymptotic constant values after ~ 30 iterations.

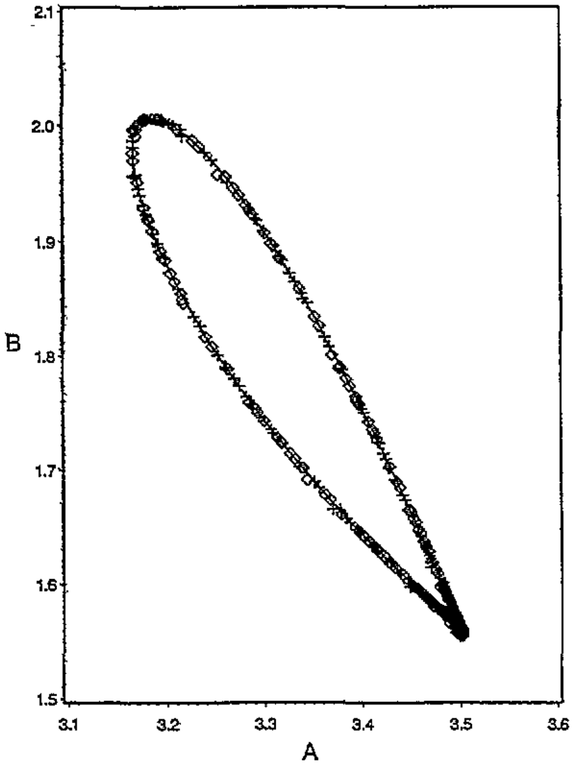

Figure 6. Phase space plot of pairs a_n, b_n^2 (denoted by $\diamond$) and a_n, b_{n-1}^2 (denoted by $+$). The solid line is obtained from (18) and (19).

The local density of states corresponding to the initial ket u_0 can be obtained directly from the continued-fraction representation of the Green's function in terms of the coefficients a_n and b_n. Thus, the information about the location of bound states can be obtained either from the density of states or from the anomalous behaviour of the coefficients in the asymptotic region. Each set of coefficients is calculated at a fixed value of K and the information obtained in this way can then be combined to show the dispersion curve for the bound-state branches. The method can be applied to the general Hamiltonian in (1) as it does not require the model to be integrable.

3. Results

Consider first the $S = 1$ Heisenberg model at $K = \pi$. The coefficients obtained using the initial choice of ket $u_0 = |K; 1, 0\rangle$ are shown in figure 7. The coefficients approach constant values asymptotically but exhibit two separate sets of deviations, both of which are due to the limitations of the computer system used to calculate them. These deviations indicate the presence of two bound states below the continuum at this value of K. This interpretation is confirmed by calculating the density of states using 500 coefficients and a constant termination procedure. Figures 8 and 9 show the results for two different energy ranges.

The two bound states are clearly visible and located at $E = 1.19, 1.27$ whereas the continuum of scattering states extends from $E = 1.408$ to $E = 6$. The continuum is

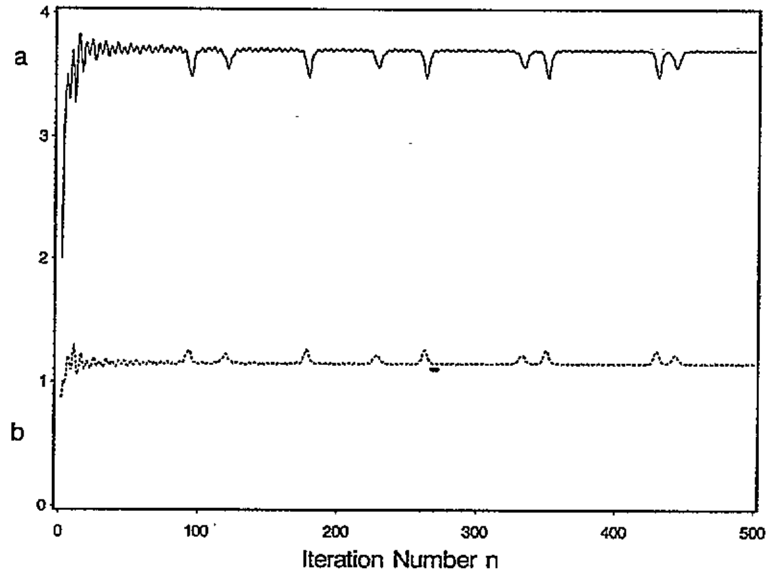

Figure 7. Double-precision coefficients a_n, b_n for the $S = 1$ Heisenberg model at $K = \pi$.

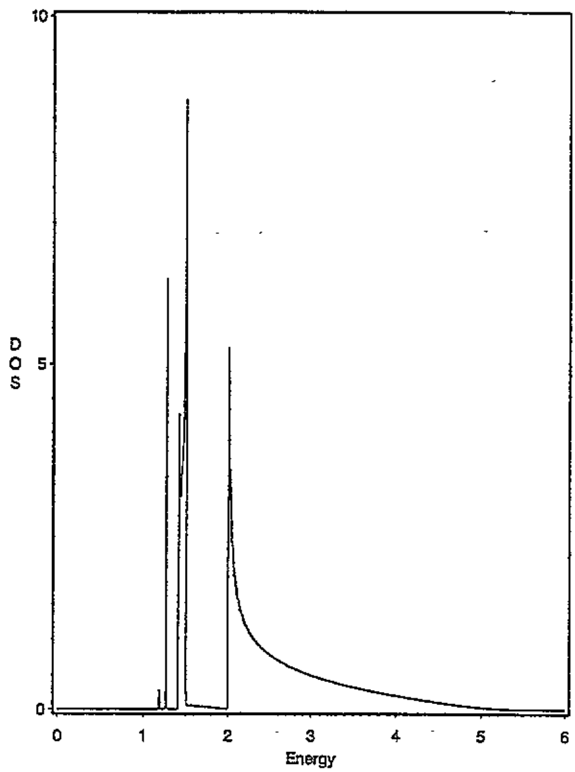

Figure 8. Three-magnon density of states (DOS) of the $S = 1$ Heisenberg model at $K = \pi$, below and over entire continuum.

composed of overlapping three free and two bound/one free contributions and the edges of

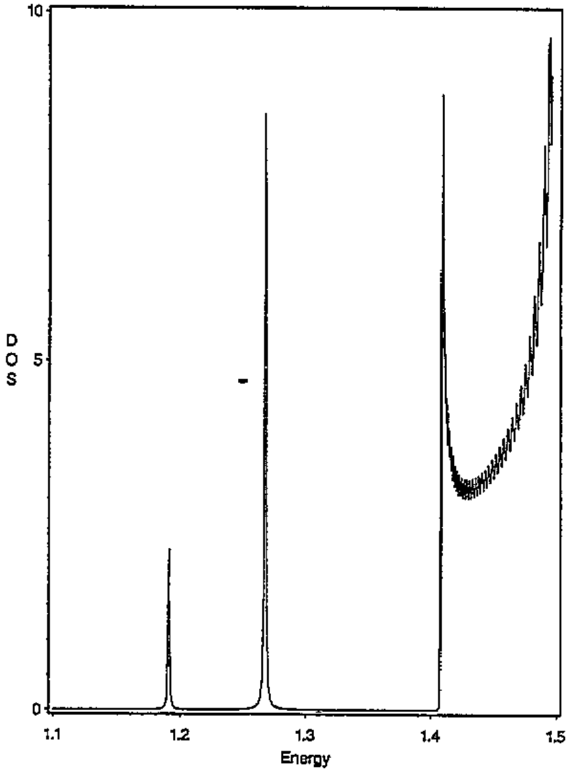

Figure 9. Three-magnon density of states (DOS) of the $S = 1$ Heisenberg model at $K = \pi$, below and inside lower end of the continuum.

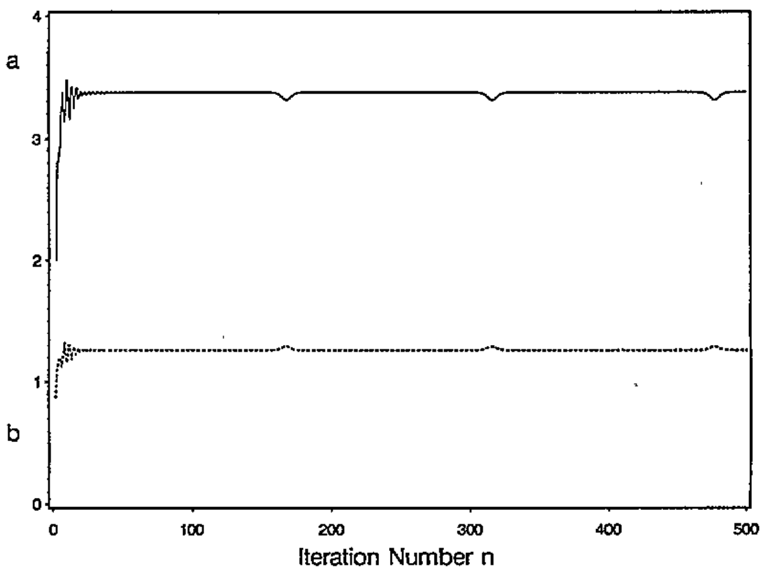

Figure 10. Double-precision coefficients a_n, b_n for the $S = 1$ Heisenberg model at $K = 0.75\pi$.

these separate continua are visible in the density of states as internal Van Hove singularities.

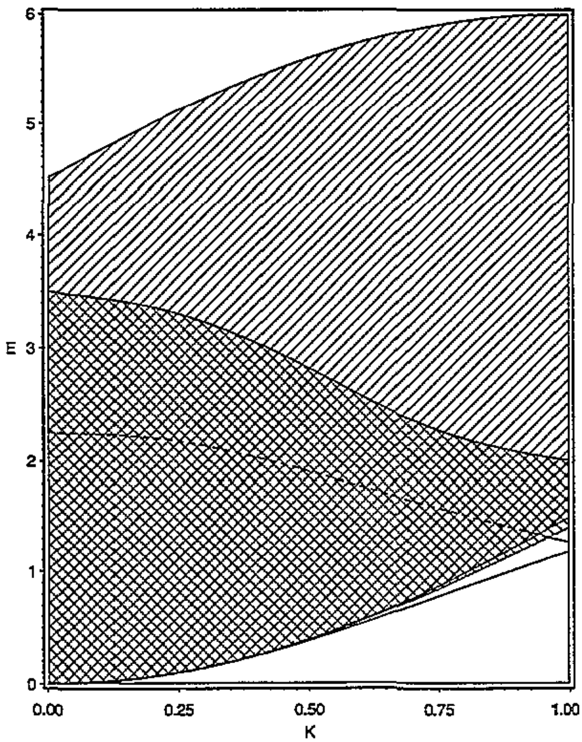

Figure 11. Three-magnon spectrum of the $S = 1$ Heisenberg model. The energy is in units of α_1 and K is in units of π. The shaded region indicates the various scattering-state continua, the solid lines outside this region are bound states, and the dashed line inside this region indicates a resonance.

Our results are in accord with those found by Millet and Kaplin [18] for $S = 1$. For smaller values of K, the upper bound state moves up in energy and eventually enters the continuum. The lower bound state moves down in energy and always remains below the continuum down to $K = 0$. The disappearance of the upper bound state can be seen directly in the coefficients. Figure 10 shows the recursion coefficients at $K = 0.75\pi$ where it is evident from the asymptotic behaviour that only one bound state remains.

The general features can be summarized by plotting the bound-state energies against K across the Brillouin zone as in figure 11. When the bound state enters the continuum, it becomes a resonance and the density of states exhibits a peak at this energy. The resonance is represented by the dashed line and the bound states by the solid lines. The continuum is indicated by the shaded region. The two bound/one free continuum determines the lower edge for all K whereas the three free continuum determines the upper edge.

These results for the $S = 1$ Heisenberg model correspond to the value of $g_2 = 1.5$ as given by (6) and are independent of g_3 since the unphysical ket with three deviations on the same site decouples from the rest. As the value of g_2 is changed towards that of the SU(2) integrable model in (5), $g_2 = (4S - 1)/(2S - 1)$, the gap between the upper and lower bound states at $K = \pi$ goes to zero and the resonance inside the continuum sharpens up into a delta function. The position of the bound states both inside and outside the continuum agree with those obtained using the Bethe *ansatz* [11]. This behaviour agrees with the conjecture of Haldane that the bound state is completely decoupled from

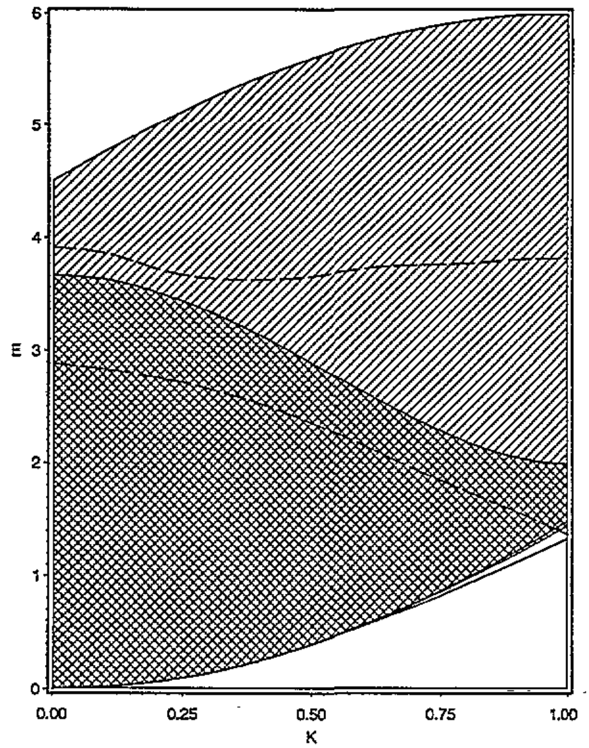

Figure 12. Three-magnon spectrum of the $S = \frac{3}{2}$ Heisenberg model. The energy is in units of α_1 and K is in units of π. The shaded region indicates the various scattering-state continua, the solid lines outside this region are bound states, and the dashed lines inside this region indicate resonances.

the continuum for this special value of g_2. For this integrable model, there are two separate two bound/one free continua corresponding to the upper and lower two-magnon bound-state branches [19]. These continua overlap the three free continuum completely and thus determine both the upper and lower edges of the scattering-state solutions.

For larger values of S, the details of the spectrum will depend on the value of g_3 as well. Figure 12 shows the spectrum for the $S = \frac{3}{2}$ Heisenberg model. There are two bound states below the continuum near $K = \pi$ with the upper branch becoming a resonance at smaller K. However, there is an additional resonant peak at higher energies across the entire zone. Figure 13 shows the spectrum for the $S = \frac{3}{2}$ integrable model where g_2, g_3 have the values in (5). The resonances sharpen up as these values are approached and the highest resonance moves up in energy and eventually lies entirely above the continuum. The upper branch of the lower bound state exists both below and above the continuum and passes right through it. The energies of the three bound-state branches completely agree with the Bethe *ansatz* values obtained by Haldane.

The three-magnon bound states form a continuous branch over min(3, $2S$) zones and are completely decoupled from the three-magnon continua if and only if

$$g_2 = \frac{4S-1}{2S-1} \qquad g_3 = \frac{6S^2-6S+1}{2S^2-3S+1}.$$

Changing either g_2 or g_3 away from these special values produces gaps between the bound-state branches at $K = 0, \pi$ and broadens the branch inside the continuum into a resonance.

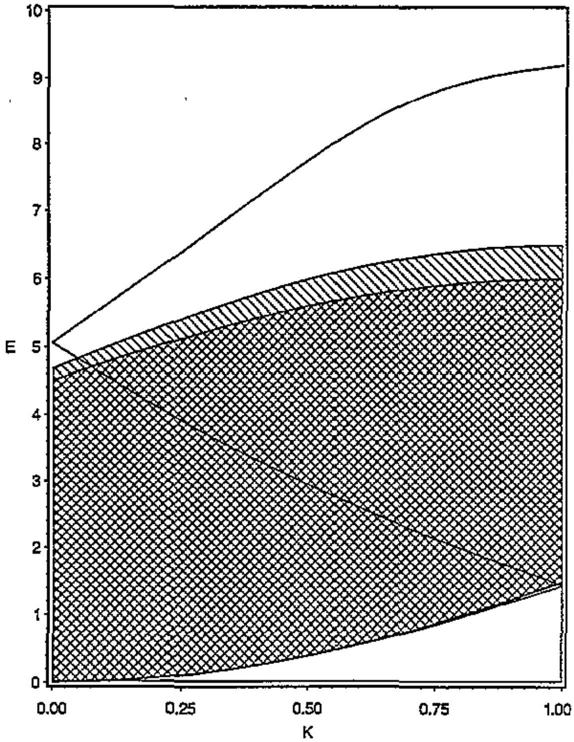

Figure 13. Three-magnon spectrum for the $S = \frac{3}{2}$ integrable model. The energy is in units of α_1 and K in units of π. The solid lines are bound states and the shaded region is the scattering-state continuum.

Our approach can be used to study the nature of the excitations for any values of S and the g_m. In the general case, with $S \geqslant 1$, the bound states and the continua interact to produce resonances inside but there are two bound states below the continua near $K = \pi$. These states are separated by a gap which decreases as S increases.

4. Summary

We have used the recursion method to obtain information about the nature of three-magnon excitations in general S-spin chains. Special features of the excitations are associated with the integrable models. The method could also be used without difficulty to study systems with uniaxial anisotropies in the Hamiltonian and higher m-magnon excitations as well.

Experimental observation of these excitations by direct measurement does not appear to be easy. Torrance and Tinkham [27] have observed multi-magnon bound states in a $S = \frac{1}{2}$ linear chain compound. They explained the experimental results using a model with both a longitudinal and transverse anisotropy in the exchange interaction. The transverse anisotropy leads to a coupling between different m-magnon excitations which allows the three-magnon bound state to be excited by photon absorption. Our results could be used a starting point for a more detailed analysis of the effects of transverse anisotropies in the exchange terms.

Acknowledgments

This work was supported by the Natural Sciences and Engineering Research Council of Canada. Two of the authors (BWS) and (DAL) also acknowledge the support of NATO under Research Grant No 0087/87.

References

[1] Bethe H A, 1931 *Z. Phys.* **71** 205
[2] Schrödinger E 1941 *Proc. R. Irish Acad. A* **47** 39
[3] Sutherland B 1975 *Phys. Rev.* B **12** 3795
[4] Izyumov Yu A and Skryabin Yu N 1988 *Statistical Mechanics of Magnetically Ordered Systems* (New York: Plenum) pp 197–295
[5] Takhtajan L A 1982 *Phys. Lett.* **87A** 479
[6] Babujian H M 1982 *Phys. Lett.* **90A** 479
[7] Parkinson J B 1988 *J. Phys. C: Solid State Phys.* **21** 3793
[8] Batchelor M T and Barber M N 1990 *J. Phys. A: Math. Gen.* **23** L15
[9] Haldane F D M 1983 *Phys. Lett.* **93A** 464
[10] Wortis M 1963 *Phys. Rev.* **132** 85
[11] Haldane F D M 1982 *J. Phys. C: Solid State Phys.* **15** L1309
[12] Chubukov A V and Khveschenko D V 1987 *J. Phys. C: Solid State Phys.* **20** L505
[13] Majumdar C K 1970 *Phys Rev.* B **1** 287
[14] Majumdar C K 1972 *J. Math. Phys.* **13** 705
[15] Mukhopadhyay S K and Majumdar C K 1976 *J. Math. Phys.* **17** 478
[16] Van Himbergen J E 1977 *Physica* A **86** 93
[17] Faddeev L D 1961 *Sov. Phys.–JETP* **12** 1014
[18] Millet P J and Kaplan H 1974 *Phys. Rev.* B **10** 3923
[19] Southern B W, Liu T S and Lavis D A 1989 *Phys. Rev.* B **39** 12160
[20] Medved A J M, Southern B W and Lavis D A 1991 *Phys. Rev.* B **43** 816
[21] Haydock R 1980 The recursive solution of the Schrödinger equation *Solid State Physics* vol 35 (New York: Academic) p 215
[22] Hodges C H 1977 *J. Physique Lett.* **38** L187
[23] Magnus A 1979 Recurrence coefficients for orthogonal polynomials on connected and non-connected sets *Proc. Conf. on Padé Approximation and Its Applications (Antwerp, 1979) (Springer Lecture Notes in Mathematics 765)* (Berlin: Springer)
[24] Turchi P, Ducastelle F and Tréglia G 1982 *J. Phys. C: Solid State Phys.* **15** 2891
[25] Toda M 1981 *Theory of Non-Linear Lattices (Springer Series in Solid-State Sciences 20)* (Berlin: Springer)
[26] Nuttall J and Singh S R 1977 *J. Approx. Theory* **21** 1
[27] Torrance J B and Tinkham M 1969 *Phys. Rev.* **187** 587, 595